Journal of the European Ceramic Society 19 (1999) 2097–2109

PII: S0955-2219(99)00028-X
0955-2219/99/$ - see front matter

Crack Propagation Studies of Thermal Barrier Coatings Under Bending

Ashok K. Ray* and Rolf W. Steinbrech

Institut fur Werkstoffe der Energietechnik -1, Forschungszentrum, D-52425 Jülich, Germany

(Received 10 November 1998; accepted 12 January 1999)

Abstract

The trends recently observed in crack propagation studies under bending for thermal barrier coatings (TBCs) in power plant application are highlighted in this paper. These studies described were performed with plasma sprayed zirconia bonded by a MCrAlY layer to Ni-base superalloy. Such thermal barrier composites are currently considered as candidate materials for advanced stationary gas turbine components. The crack propagation behaviour of the ceramic thermal barrier coatings (TBCs) at room temperature, in as received and oxidized conditions reveals that cracks grow linearly in the TBC with increase in bending load until about the yield point of the superalloy is reached. Approaching the interface between the ceramic layer and the bond coat, a high threshold load is required to propagate the crack further into the bond coat. Once the threshold is surpassed, the crack grows rapidly into the brittle bond coat without an appreciable increase in the load. At a temperature of 800°C, the crack is found to propagate only in the TBC (ceramic layer), as the ductile bond coat offers an attractive sink for stress relaxation. Effects of bond coat oxidation on crack propagation in the interface regime have been examined and are discussed. © *1999 Elsevier Science Limited. All rights reserved*

Keywords: thermal barrier coatings, mechanical properties, ZrO_2, engine components, crack propagation.

1 Introduction

Research on evaluating the lifetime and thermo-mechanical behaviour of candidate materials in turbine blades which are made of superalloys with ceramic thermal barrier coatings has gained increasing interest in recent years. To cater to the needs of the industry, crack initiation and propagation studies in thermal barrier coated Ni-base superalloys having a γ' phase > 50% is an important area of research to evaluate the lifetime of the TBC superalloys used as gas turbine components in power plant applications. These superalloys are the standard material for hot stages of gas turbines where blades and vanes are subjected to high mechanical stresses and aggressive environments.

The nickel-base alloys which have been developed for this application are constituted of a γ matrix (solid solution based on nickel) strengthened by both solid solution and precipitation of the γ'-Ni_3 (Ti,Al) phase. The demand for higher efficiencies and durability has resulted in directionally solidified alloys, single crystals, alloys strengthened by oxide dispersion (ODS) or by carbide fibres.[1] Crack propagation studies and failure of TBCs on Ni-base superalloy having a γ' phase > 50% under bending for gas turbine vanes have been studied and reported elsewhere.[2]

TBCs represent an attractive materials approach of enhancing the high temperature limits for systems such as gas turbines, aircraft engines and diesel engines. However, the significant differences in properties between ceramic and metal, as well as the severe temperature gradients applied in such systems, cause thermal stresses that can lead to cracking, delamination and ultimately spalling of the coating. It was established under conditions that simulate jet engine applications[3,4] that one significant contributor to such spalling is oxidation of the bond coat. Many studies have concentrated on the time to spalling as a function of heat flux[5–8] and as a function of surface stresses and crack tip opening.[8]

Plasma-sprayed yttria stabilized zirconia (PSZ) is currently the most advanced system envisaged for thermal barrier coatings to be applied on hot turbo

*To whom correspondence should be addressed present address: National Metallurgical Laboratory, Jamshedpur-831007, Bihar, India; fax: +91-657-426527; e-mail: asokroy@csnml.ren. nic.in

engine components. Although this system is known for its excellent thermomechanical resistance at elevated temperatures, the relationship between performance and microstructure of such complex coatings is not fully understood.[9] Particular attention has been paid to the microstructure evaluation of the ceramic/bond coat interface and to the Al_2O_3 scale developed on the bond coat under oxidizing conditions. The morphology of the dense Al_2O_3 scale changes from the bond coat to the ceramic. These observations,[9] also give valuable insights into the temperature situation at the interface and are expected to allow in future a more accurate formulation of a relationship between temperature, phase content and coating life time.

The insulation properties of the ceramic coatings provide:

- an increase in the thermal inertia of the parts and therefore a reduction of the severe thermal temperature gradients during heating and cooling of the gas turbine components (i.e. improvement of the thermal fatigue behaviour).
- a reduction of the substrate temperature and therefore the possibility of increasing the turbine inlet temperature and/or decreasing the cooling air mass flow (efficiency gain in both cases).

Zirconia partially stabilized by 6–8 wt% yttria seems to be a reasonable material solution in this respect at the present time.[1] In addition, a NiCrAlY or NiCoCrAlY type metallic undercoat insures the bonding and the adherence of the thermal barrier on the substrate and also improves the coating corrosion resistance. In fact, thermal barriers are mainly used to solve difficulties related to high temperature: it has been shown[1] that their behaviour in a corrosive environment especially in the presence of vanadium is not entirely satisfactory. But, taking into account that the thickness of the thermal barrier is about 400–500 μm, it is clear that given the incidence of such thickness on the geometry of the engines, the coating studies must be carried out very early, in fact simultaneously with the conception of the component life. These overlay coatings, as a newer development, were specifically designed to meet minimum mechanical performance as well as improved environmental protection. The major attraction of the overlay coatings is some flexibility in composition, which in many cases allow tailor made solutions. However, some restrictions exist from the deposition technique and from the deposition substrate. At high temperatures, the interdiffusion processes[1] between the bond coat and substrate may be very important and, in extreme cases, lead to a rapid degradation of coating properties (systems with low compatibility, for example Co-base coating on Ni-base superalloy: at high temperature rapid diffusion of Al from Co-base coating on Ni-base superalloy with formation of an intermediate brittle intermetallic layer).

The coating plays its protective role if it is able to resist mechanical stresses that may induce cracking and spalling. The sources of mechanical degradation to which the coating may be submitted are (a) stresses applied to the component (thermomechanical cycles), (b) stresses resulting from the thermal expansion mismatch between substrate and coating and (c) adventitious causes such as erosion, impact. It is then important to consider the intrinsic mechanical properties of coatings such as ductility and thermal expansion coefficient; depending upon the thermomechanical cycles, these properties will define the coating behaviour.

In studying the life of the TBCs, consequently in recent years, more concentrated efforts have been made in studying the mechanisms of crack initiation and propagation in TBCs under controlled experimental conditions.[8–10] Keeping this in view, an attempt was made to study the crack propagation behaviour in TBCs at room temperature in the as-received and oxidized conditions as well as at a higher temperature (800°C).

2 Experimental

The failure behaviour of the TBC systems was studied in bending tests with in situ observation of the cracking mechanisms.

2.1 Material specification

Ni-base superalloy (Inconel-617) from indigenous source was the substrate material for the TBCs. A NiCrA1Y type metallic undercoat or bond coat was first generated by plasma spaying to insure the bonding and the adherence of the thermal barrier on the substrate and to improve the corrosion resistance of the TBC Thereafter, zirconia (stabilized with 8 wt% yttria) based thermal barrier coating was plasma sprayed on the bond coat. Before initiation of the plasma spray, the substrate was treated through reverse transferred arc sputtering to remove any traces of oxide that may have formed during preheat. The coating distribution is determined by computer-controlled gun and part motion. Typical parameters for turbine vane coating[11] would have a gun–substrate distance ~40–70 mm at a chamber of 30–60 torr (0·004–0·008 MPa); a gun operating at 80 kW with powder feed rate of around 4 kgh^{-1}. The TBC substrate for the gas turbine vane produced was used as the material in the present investigation.

2.2 Specimen preparation

From the as received plate-shaped vane components four-point bend (FPB) specimens were machined using ultrasonic cutting and spark erosion technique. The height (h), width (b) of the various FPB specimens, along with the thickness of the ceramic layer (d_c) and the thickness of the bond coat (d_b) are listed in Table 1. Figure 1(a) shows a schematic cross sectional view of the multi layered specimens.

2.3 Microstructure

The as received TBC-substrate specimens were first mounted using standard thermosetting resins and then polished manually on emery polishing paper of different grits (200, 400, 800 and 1200). This was followed by polishing the mounted specimens with 9, 6, 3 and then 1 μm alumina suspension in *master make* solution, cleaning with acetone and drying the specimens. The thickness of the TBC (ceramic layer) as well as that of the bond coat were measured by optical microscopy. Another set of samples were oxidized at 1000°C for 200 h in an Argon/20 vol% oxygen atmosphere. Prior to the crack propagation tests under four point bending all the samples were polished using a final polishing step with 0·1 μm diamond paste. The surface was carefully cleaned with acetone and dried. After the FPB tests, the microstructure of the substrate was examined by electrochemically etching the specimens. To reveal the triple point junction (i.e. the grain edges at the junction of adjacent grain boundaries and the grain boundary precipitates) of the superalloy Inconel-617 in Type2 specimen, 35 ml H_2SO_4, 40 ml H_3PO_4 and 25 ml H_2O was the electrolyte (2 V). Typical optical micrographs of the specimens in both unetched and etched conditions are shown in Figs 1(b)–2(d).

2.4 Crack propagation studies

Crack propagation studies were conducted under four-point bend (FPB) loading using a miniature testing device monitored on the stage of an optical microscope (room temperature (RT) tests) and an servohydraulic Instron-1362 machine (800°C test). The TBC (ceramic layer) was on the tensile surface. The ramp rate for loading was maintained as 2·5 Ns^{-1} and the deflection was measured with an LVDT. The load versus deflection curves [Fig. 3(a) and (b)] were recorded as the raw data from each experiment. Most tests were conducted at room temperature (RT = 25°C), where the bond coat behaves brittle and few at 800°C where the bond coat is ductile. Strain values corresponding to deflection were evaluated on the basis of geometric two layer relations using the following equations:[12]

$$\varepsilon = h_o/R \tag{1}$$

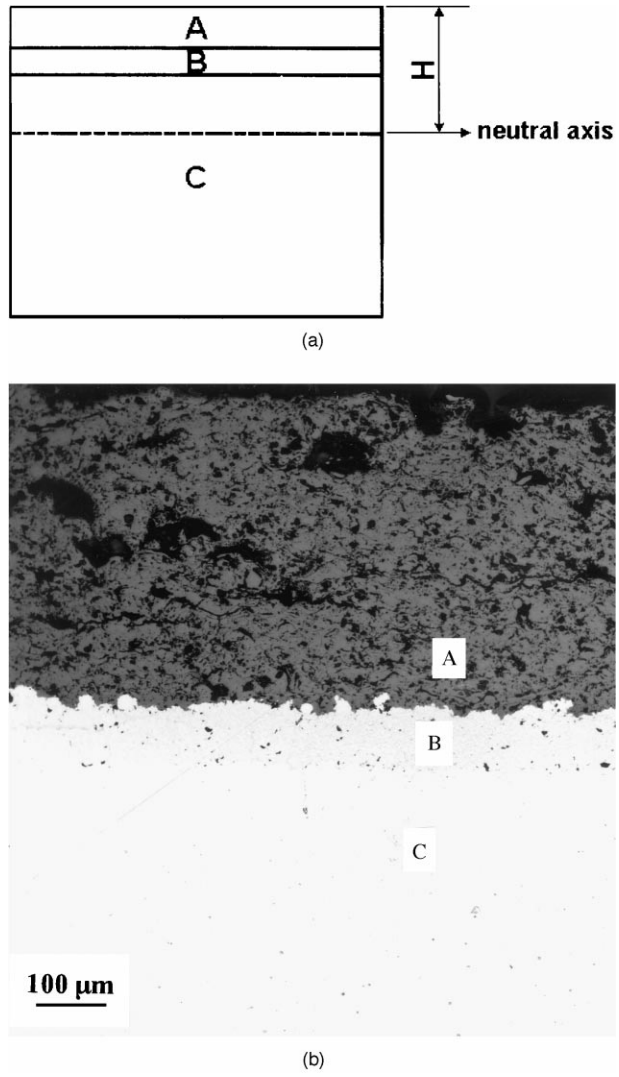

Fig. 1. (a) Schematic of cross-sectional view of a plasma sprayed TBC on Ni-base superalloy: A, TBC (ceramic layer); B, bond coat; C, substrate (Ni-base superalloy); H, distance of neutral axis from the surface of the TBC. (b) Micrograph of a plasma sprayed TBC in as-received condition (type1). The sample is polished and unetched. The TBC (ceramic layer) possesses pores as processing defects incorporated by the plasma spraying process. The bond coat is also found to possess a lot of porosity as processing defect. A, TBC (ceramic layer); B, bond coat; C, substrate.

Table 1. Dimension and coating thickness of the TBC specimens for FPB (four-point bend) experiments

Type	*Test temperature (°C)*	h *(mm)*	b *(mm)*	d_c *(mm)*	d_b *(mm)*
1. As-received	25 (RT)	1·83	2·61	0·50	0·10
2. Oxidized at 1000°C for 200 h	25 (RT)	2·41	2·22	0·30	0·10
3. As-received	800	3·00	3·88	0·50	0·20

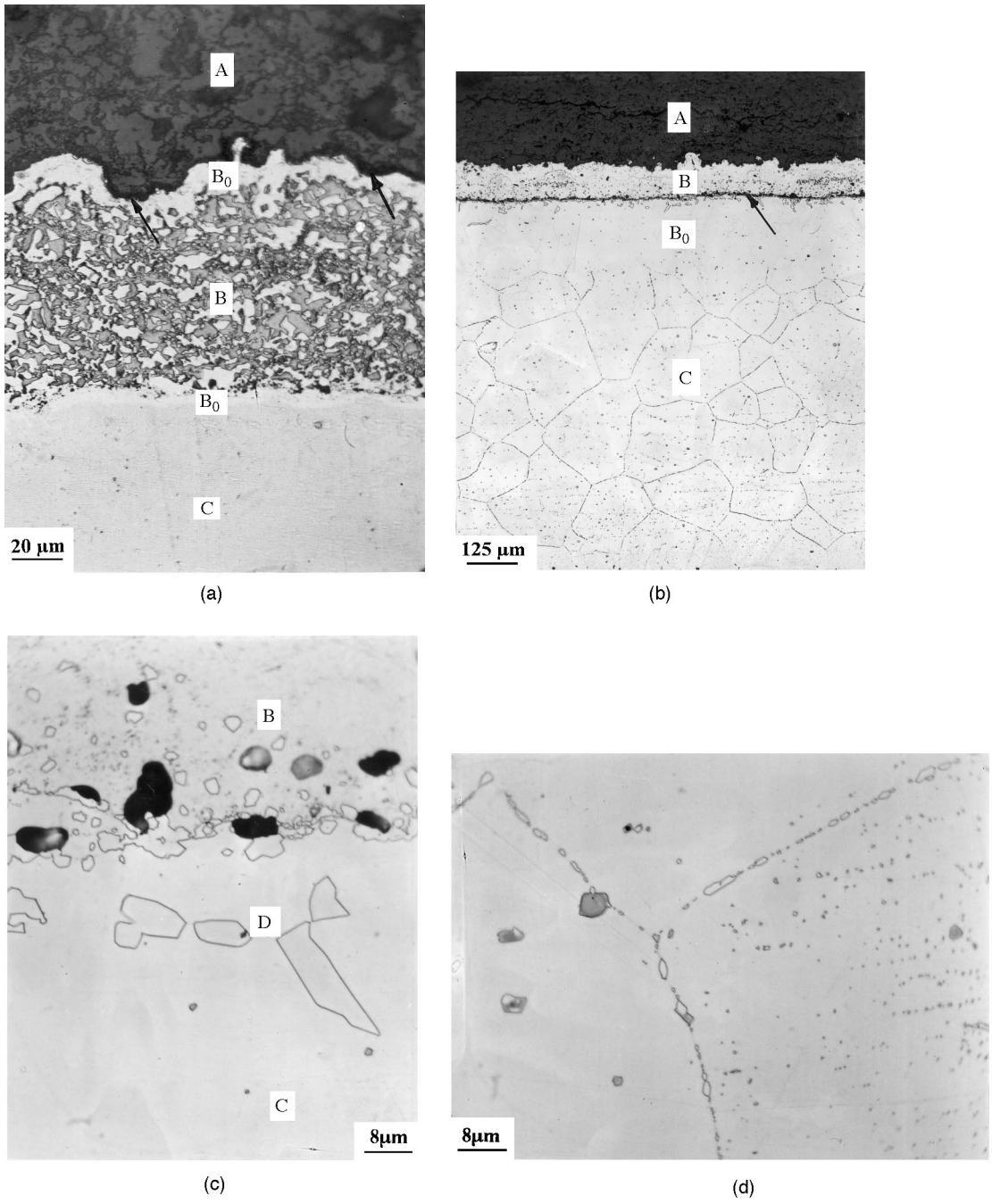

Fig. 2. Micrograph of the oxidized specimen (type2). Arrow indicates the Al_2O_3 layer of $\sim 2\,\mu$m thickness:[2] A, TBC (ceramic layer); B, bond coat; B_0, Al-depleted zone; C, substrate. (b) Micrograph of oxidized specimen (type2) at a low magnification. Al-depleted zone is seen after the bond coat. Arrow indicates carbide precipitation which is seen at the interface of bond coat and substrate. Note also the carbide precipitation within the coarsened grains in the substrate.[2] A, TBC (ceramic layer); B, bond coat; B_0, Al-depleted zone; C, substrate. (c) Micrograph of the oxidized specimen (type2) at a high magnification. A lot of porosity existed in the bond coat. Carbide precipitation is seen in region D, i.e. at the interface of bond coat/substrate:[2] B, bond coat; C, substrate. (d) Micrograph of the substrate material oxidized at 1000°C for 200 h (type2). The triple point junction is clearly marked by the carbide precipitation of secondary carbides. Primary carbides are seen inside the grains.[2]

$$R = \delta/[1 - \cos(\theta/2)] = \delta/1\{1 - \cos[\sin^{-1}(\delta/L/2)]\} \tag{2}$$

where ε is the strain corresponding to deflection δ, L is the difference between the outer and inner span in four point bend loading, h_o is the distance of the neutral axis of the FPB specimens from the interface of the ceramic coating and the bond coat. R is the radius of curvature of the neutral axis due to deflection at an angle θ. h_o is calculated from the following expression:[12]

$$h_o = E_s d_s^2 - E_c d_c^2/(2E_s d_s + 2E_c d_c) \tag{3}$$

where $E_s = 210$ GPa and $E_c = 110$ GPa.[2] E_s and E_c are the elastic moduli of the substrate and TBC (the ceramic layer), respectively, d_s and d_c are the thickness of the substrate and the ceramic layer,

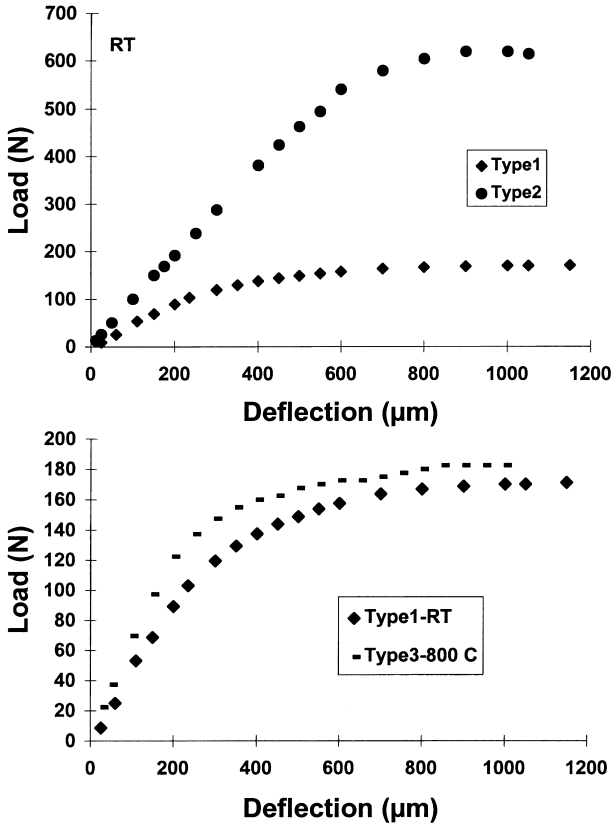

Fig. 3. (a) Load versus deflection curves for composite beam specimens, type1 and type2. (b) Load versus deflection curves for composite beam specimens, type1 and type3.

respectively. It important to note that in this first order approximation, the subtle differences in the elastic properties between the bond coat and the substrate were neglected.

The load versus strain and stress versus strain curves of the composite beam specimens are shown in Figs 4 and 5. Variation of crack length with load and deflection are shown in Fig. 6(a)–(f).

The TBC inherited many microcracks due to the plasma spraying process, but under bending stresses bigger cracks became prominent and grew across the height thickness of the specimen. The crack length was monitored microscopically on the side surface of the specimens and was measured with special care in locating the crack tip. The crack path trajectory was recorded and printed by a video scanner for RT tests and by a sophisticated camera system attached to the microscope for the high temperature (HT = 800°C) test. The crack extension was correlated to the applied load and corresponding deflection of the composite. Load versus crack length plots [Fig. 6(a)–(c)], and deflection versus crack length plots [Fig. 6(d)–(f)] were generated. Subsequently, these deflection values were plotted against their corresponding load values by a best fit polynomial of the form $y = A + Bx + Cx^2 + Dx^3$ and by resorting to the integral method, the values of the energy, $U = \int Ydx$

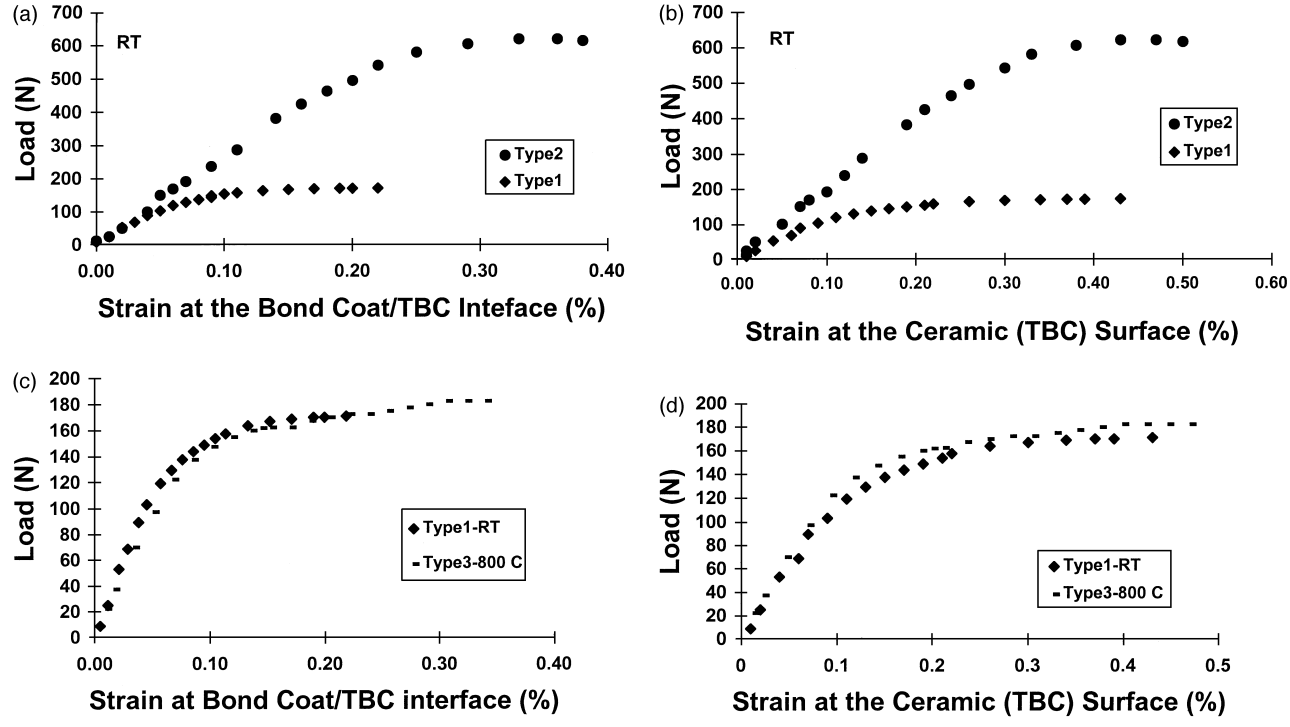

Fig. 4. (a) Plots of load versus strain at the interface of bond coat/TBC for composite beam specimens, type1 and type2. (b) Plots of load versus strain at ceramic (TBC) surface for composite beam specimens, type1 and type2. (c) Plots of load versus strain at the interface of bond coat/TBC for composite beam specimens, type1 and type3. (d) Plots of load versus strain at ceramic (TBC) surface for composite beam specimens, type1 and type3.

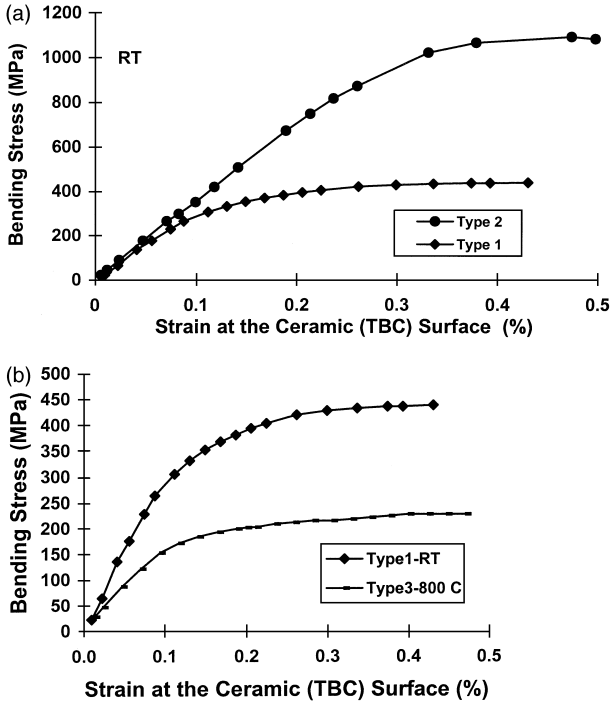

Fig. 5. (a) Stress versus strain curves for composite beam specimens, type1 and type2. (b) Stress versus strain curves for composite beam specimens, type1 and type3.

were evaluated corresponding to each deflection values, enabling raw data plots of U versus a (crack length). The slope at the various points corresponding to the crack lengths when normalized with respect to the height of the specimen gave the strain energy released with respect to crack extention during bending. The strain energy values released at the interface of the ceramic coating and the bond coat and within the bond coat are shown in Table 2.

3 Results and discussion

3.1 Metallographic studies

A micrograph of plasma sprayed TBC substrate (Type1) is shown in Fig. 1(b). It reveals that the TBC possessed a lot of processing defects like pores (~18–20% porosity) in Type1 specimen. Further, it was evident that the bond coat also possessed a lot of porosities as defects incorporated from plasma spraying. An Al-depleted zone just below the TBC along the TBC/bond coat interface as well as at the bond coat/substrate interface was observed in Type2 composite beam specimen [Fig. 2(a)]. Similar observations were also made by previous investigators in studying the oxidation behaviour of sprayed MCrAlY coatings in air as well as in helium with 1% O_2 at 1050°C.[13] They have observed Al depleted zone below the bond coat and also below the TBC after a long time oxidation of 500 h.

The bond coat/substrate interface revealed the presence of porosity [Fig. 2(b)] and carbide precipitations [Fig. 2(c) and (d)] in Type2 material. The metal matrix shows grain growth with carbide precipitation within the grains [Fig. 2(c)]. At a higher magnification the triple point of three adjacent grains is shown [Fig. 2(d)]. Possibly secondary carbides precipitate out along the grain boundaries and primary carbides in the center of the grains as reported in Ref. 14.

Due to the high oxygen conductivity of ZrO_2 at high temperature and the presence of porosity in the TBC and in the bond coat, the Al in the bond coat oxidizes to Al_2O_3 at the TBC/bond coat interface to about 2 μm in thickness [Fig. 2(a)]. Therefore following this interface, there is an Al depleted zone in the bond coat. It appears from Fig. 2(a) and (b) that a fraction of Al in the bond coat also diffuses into substrate. Therefore an Al depleted zone also occurs between the interface of the substrate/bond coat and the bond coat. Previous authors have also reported similar observations in such TBC substrates.[13]

3.2 Mechanical properties and crack propagation behaviour of the TBCs

For crack propagation studies, four point bending was chosen as in gas turbines, the blades and vanes are often subjected to bending.

If a homogeneous rectangular beam is subjected to symmetrical bending,[15] the neutral axis of the beam coincides with the centroid of the cross section. However, if one of the beam's surfaces is coated with a material of different elastic modulus, the beam is no longer homogeneous and the neutral axis shifts from the centroid of the cross section of the composite beam. Thus an in-plane modulus of the coating was proposed from the shift of the neutral axis.[15] In the bent composite beam, the dependence of the normal stresses σ_c and σ_s (where the subscripts c and s denote the TBC and the metallic substrate, respectively) upon the transverse thickness coordinate Y (Fig. 7) can be expressed as follows:[15]

$$\sigma_c = E_c Y/R$$
$$\sigma_s = E_s Y/R \qquad (4)$$

where R is the radius of curvature of the neutral axis, and E_c and E_s are the elastic moduli of the TBC and the substrate. From the equilibrium of the axial forces, the following equation has to be satisfied:[15]

$$\int_{-h_o}^{d_s-h_o} \sigma_s \mathrm{d}A + \int_{-h_o-d_c}^{-h_o} \sigma_s \mathrm{d}A = 0 \qquad (5)$$

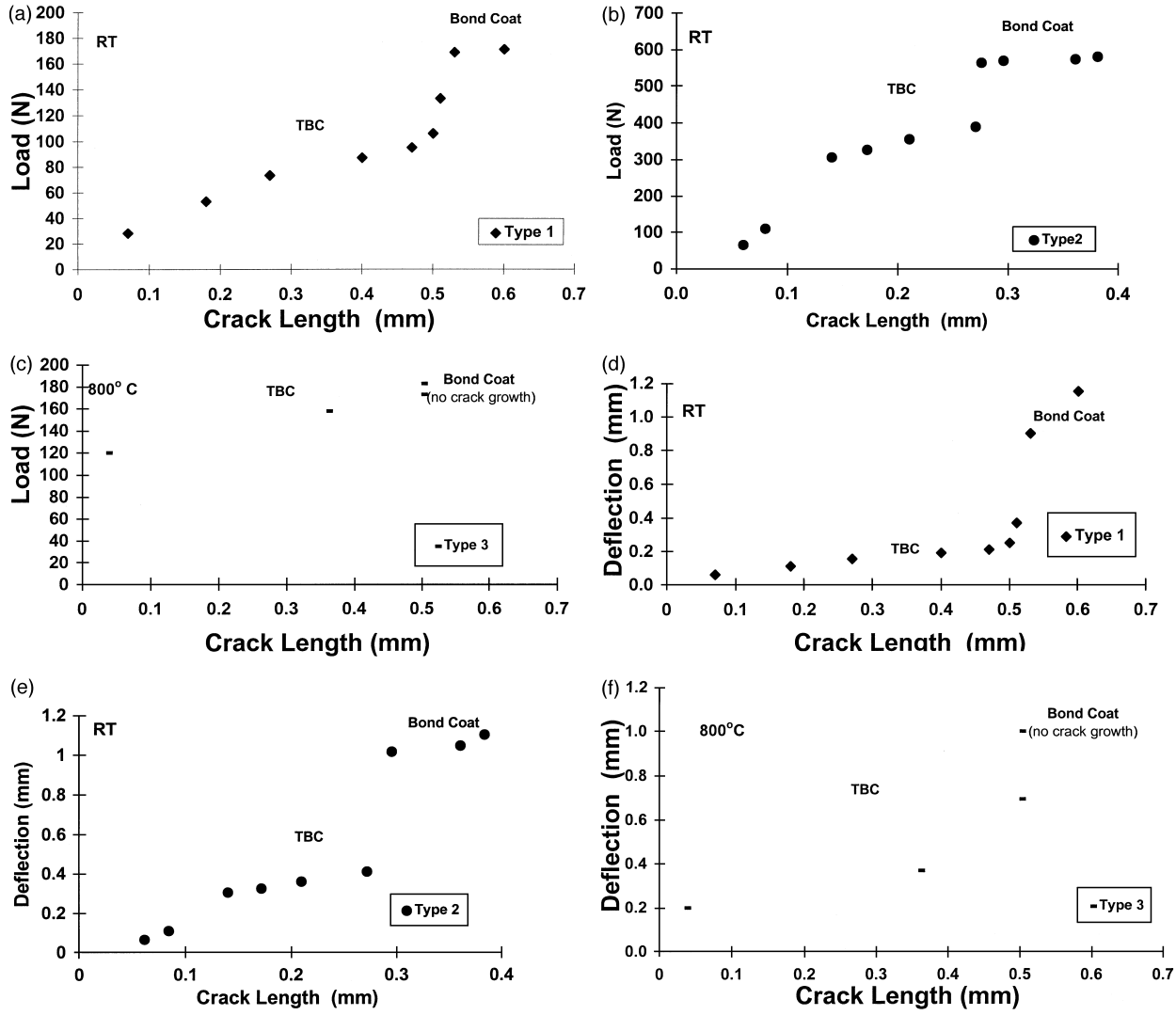

Fig. 6. (a) Plot of load versus crack length for the composite beam specimen, type1. (b) Plot of load versus crack length for the composite beam specimen, type 2. (c) Plot of load versus crack length for the composite beam specimen, type3. (d) Plot of deflection versus crack length for the composite beam specimen, type1. (e) Plot of deflection versus crack length for the composite beam specimen, type2. (f) Plot of deflection versus crack length for the composite beam specimen, type3.

Table 2. Strain energy values at the interface of bond coat and TBC and in the bond coat of the FPB composite specimens

Type	*Test temperature, (°C)*	*Strain energy released (J cm^{-2})*		*% Strain at the interface of bond coat/TBC*
		At the interface of bond coat/TBC	*Within the bond coat*	
1. As-received	25 (RT)	131	23·07	~0·1
2. Oxidized at 1000°C for 200 h	25 (RT)	170	17·60	0·2
3. As-received	800	5·40	—	0·34

where A is the cross-sectional area. Substituting eqn (4) into eqn (5) yields h_o as given in eqn (3). However, for calculation of strain in the ceramic layer, H was taken into consideration instead of h_o, where

$$H = h_o + d_c \tag{6}$$

The strain at the TBC (the ceramic layer) and at the interface between bond coat/TBC are displayed for as received (RT test), oxidized condition (RT test) and at high temperature (800°C) test (Fig. 4). The results are compatible with those reported for similar TBCs in bend tests.[1–7]

Taking into account the relative mechanical properties of the superalloy and the coating, the latter has a low strength due to the numerous defects and a lower elastic modulus and the system alloy + coating can be considered as a composite in which the load bearing contribution of the coating is negligible.[1] If the coating formation involves consumption of alloys as in the case of aluminides and induces a reduction of alloy section, it is

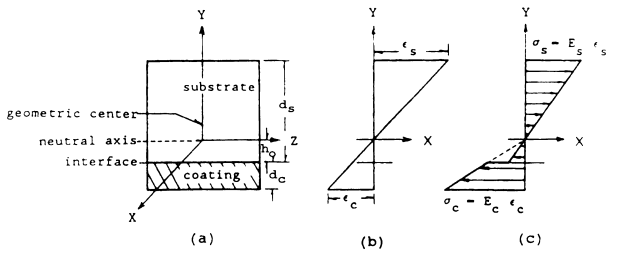

Fig. 7. Stress/strain relationship in a composite beam subjected to a pure bending moment: (a) cross-section of the composite beam; (b) strain development in the axial direction; (c) stress in the axial direction.[14]

necessary to consider the residual section of superalloy for the determination of the effective mechanical stress.[1] This is of particular importance in the case of cooled blades with thin wall sections. On the other hand, for overlay coatings as in the present case, there is no reduction in the load bearing section (eventually a very small reduction, due to interdiffusion effects during the heat treatment applied to improve adherence). These coatings introduce just an additional mass subjected to centrifugal stresses for the blades. As a point of interest, it was found,[1] that for both the types of coatings, the ratios of the total section of the component accounting for the stress due to centrifugal loads to the actual load bearing section (alloy) were found to be quite comparable. Therefore in the present investigation, it was assumed that the load is borne by the superalloy substrate and not by the coating. From the load–deflection curves of the bent composite beam, the bending stresses were evaluated without the TBC (ceramic layer) using the standard formula as per ASTM STP 410, for four point bend loading of miniature specimens. The bending stresses at the yield point were 296, 693 and 200 MPa for Type1, Type2, Type3 mateials, respectively [Fig. 5(a) and (b)]. The stress values for the as received material tested at room temperature are quite compatible to the values reported in literature for Inconel 617. It was found that the bending stress at the yield point of the oxidized specimens were about 2·3 times higher than those of the as received specimens. This could be attributed to microstructural toughening due to carbide precipitation at the bond coat/substrate interface, grain boundary precipitation and coarsening of grains in the substrate of Type2 specimen[14] as discussed in Section 3.1.

The strain energy values at the interface of the ceramic layer and the bond coat and within the bond coat as listed in Table 2 implies that for the oxidized sample a higher strain energy is required for the crack to penetrate the bond coat compared to the as received TBCs and this is also probably due to microstructural toughening of the oxidized sample as has been discussed above. Earlier work[16] had reported room temperature impact toughness of 200 J cm^{-2} for Inconel 617. Owing to the differences in the crack tip loading rates, i.e. owing to dynamic effects, the impact toughness value of Inconel 617 reported[16] at room temperature is higher than the strain energy released at the bond coat/TBC interface in monotonic loading for as received FPB composite specimens in the present investigation.

It should be noted that deformation in the TBC and that in the bond coat pertained to the elastic limit and plastic limit of the load versus deflection curves, respectively [Figs 3 and 6(a) and (b)]. Although in type3 composite beam specimen there was a huge deflection [Fig. 3(b)], the crack front never penetrates the bond coat [Fig. 6(c) and (f) and Fig. 11(a)], as the bond coat is ductile at 800°C. Therefore in the high temperature (800°C) test, since the bond coat is ductile and crack propagation is confined only to the TBC (ceramic layer), the strain energy released at the interface of bond coat/TBC was very less (5·35 J cm^{-2}) as shown in Table 2.

The mechanical integrity of the bond coat is related to its ductility. Ductility is generally quantified by the strain necessary for the initiation of the first crack in a coated material using bending or tension tests.[1] The elevated temperature tests reveal that above a certain temperature, the strain to cracking increases rapidly which means that the material behaves in a ductile way.[1] It is then possible to define a ductile to brittle transition temperature (DBTT). In the case of aluminide coatings, the DBTT ranges from 600 to about 750°C. The transition temperature depends on the thickness of the coating as well as the Al content. As far as the MCrAlY bond coat is concerned a somewhat less brittle behaviour is reported than that of aluminides,[1] but the ductility also depends on the Al content. The transition temperature which is dependent on the Al content in the bond coat, range from 200°C for low Al coatings (6–9% Al, high volume fraction of γ-phase) to 800°C for Al-rich CoCrAlY coatings (12% Al, high volume fraction β-CoAl phase) as shown in Fig. 8. When the components are subjected to severe thermomechanical cycles, MCrAlY coating is chosen because of its favorable ductility and thermal expansion coefficient. There is no really quantitative approach available to date.[1] However, since the coating composition may noticeably change as a function of time and service environment, in this instance, information drawn from service experience are ultimately needed.

For growth of stable cracks in brittle materials (e.g. ceramics, bond coat), notched and precracked specimens are usually desired. In the present

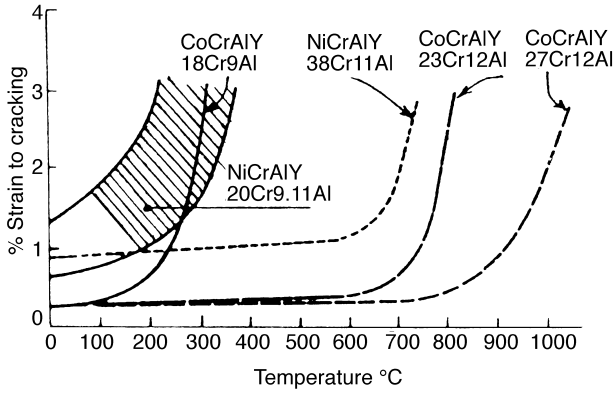

Fig. 8. Ductile to brittle transition temperature of various MCrAlY coatings.[1]

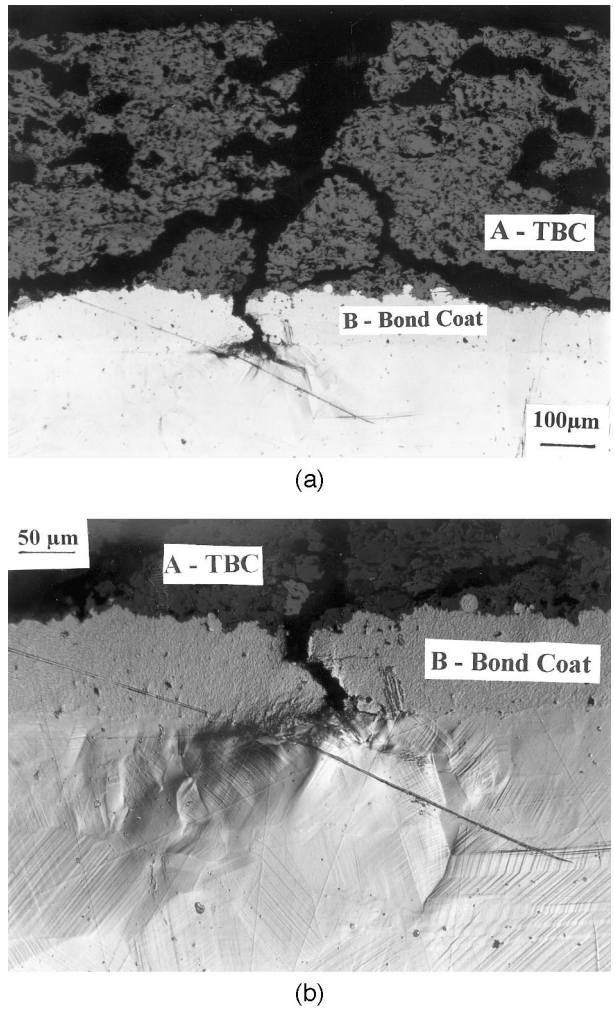

Fig. 9. (a) Crack path trajectory in the TBC (ceramic layer) and in the bond coat in crack propagation studies under bending at RT of type1 composite beam specimen. Crack branching in the TBC, crack tip blunting at the interface of bond coat/substrate and severe crack deflection in the bond coat is seen. (b) Micrograph showing several cracks in the TBC joining up (extreme right on the top) in crack propagation studies of type1 composite beam specimen, at RT. Finally the main crack penetrates the bond coat in type1 specimen. Crack tip blunting is seen at the interface of bond coat/substrate followed by a substantial amount of plastic deformation indicative of deformation twins in the substrate.

situation, the TBC (ceramic layer) already has flaws like microcracks and porosities. Application of load generates stable crack extension because several sources of energy dissipation become activated, e.g. crack deflection, crack arrest in pores, crack bridging and further microcracking. The crack path trajectory recorded and printed by a video scanner for RT tests and by a sophisticated camera system attached to the microscope for 800°C tests, are shown in Figs 9 and 10, and Fig. 11 respectively.

It is evident from Fig. 6(a)–(c), that in the present investigation for all composite beam specimens, the crack propagates linearly in the TBC with increase in the bending load till about the yield point [see also Fig. 3(a) and (b)] of the substrate. Thereafter, at the TBC/bond coat interface, a high threshold load is required [Fig. 6(a)–(c)] for the crack to propagate further in the bond coat. Once the threshold is reached, the crack propagates faster in the bond coat without an appreciable increase in the load, with almost a zero slope [Fig. 6(a)–(b)]. Deflection versus crack length curves ([Fig. 6(d)–(f)] revealed positive linear dependence of crack length with deflection in the ceramic layer as well as in the bond coat. It clearly infers that as the crack front penetrates the bond coat, there is a substantial amount of deflection with propagation of the crack within the bond coat, indicative of enormous plastic deformation ahead of the crack front at the bond coat/substrate interface [Figs 9 and 10(e)] and formation of deformation twins in the metal substrate [Figs 9(a) and 10(e)] in the RT tests. The crack front also revealed blunting of the crack tip at the bond coat/substrate interface indicative of high ductility of the material. It also implies that the crack to propagate further in the substrate requires a very high bending load. There was no spalling of the TBC for the composite beam specimen in any of the bend tests at RT and also at the high temperature (800°C) test.

It is noteworthy that the crack path trajectory in the TBC (ceramic layer) often showed crack branching [Figs 9(a) and 10] and crack deflection [Figs 10(a)–(c) and 11]. Generally for material with *R*-curve type behaviour, this is a well established phenomenon and it could partly account for the rising trend in the K_R (fracture resistance) values.[17–21] Possibly, due to the presence of porosities on the scale of grain sizes and probably due to the presence of complex residual stress field, high resistance to crack propagation was created and hence the crack tended to find a new starting point at the weakest area away from the main path. However, the crack front deflected and penetrated straight into the bond coat without any indication of crack branching. At a temperature of 800°C, the crack is found to propagate only in the TBC [Figs 6(c) and (f), and 11] as the ceramic thermal barrier coatings (TBCs) offer an attractive means

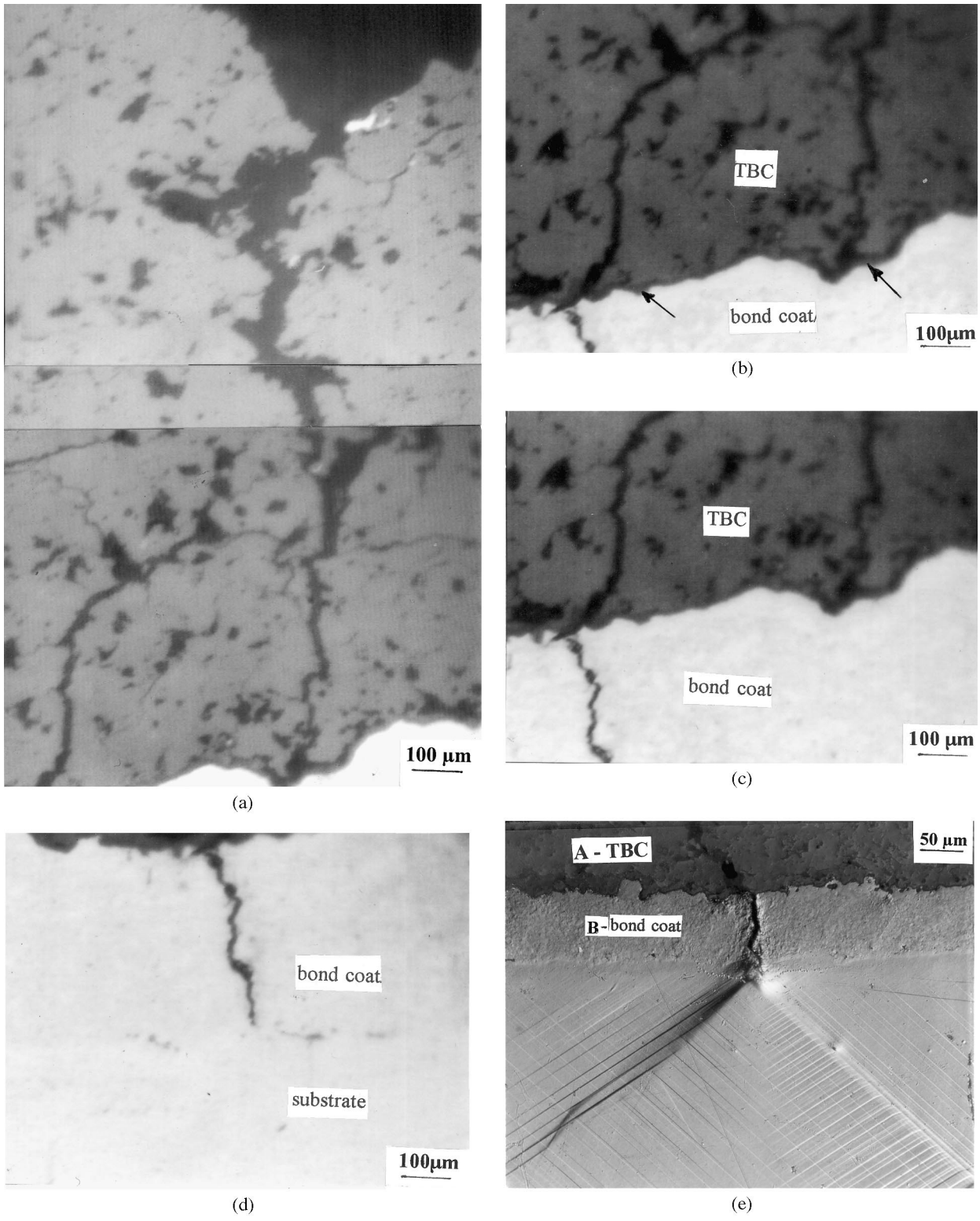

Fig. 10. Typical crack path trajectory in crack propagation studies under bending at RT for type2 composite beam specimen in heat-treated condition (oxidized at 1000°C for 200 h). (a) Crack propagation in the TBC. The crack is found to initiate from a surface pore in the TBC. The crack frequently branches in the TBC. (b) The crack front penetrates the Al_2O_3 layer at the interface of TBC/bond coat and then into the bond coat. Arrow indicates the Al_2O_3 layer. (c) Crack path trajectory in the bond coat (white portion). The dark region corresponds to the TBC. (d) Crack path trajectory till the end of the bond coat. The crack front does not penetrate the substrate. (e) Crack path trajectory in the in the bond coat in crack propagation studies at RT of type2 composite beam specimen in heat-treated condition (oxidized at 1000°C for 200 h). The crack front penetrates vertically into the bond coat from the TBC (top-most layer). The substrate reveals substantial deformation twins.

of protecting the metallic component from thermal loads and as the bond coat becomes ductile at high temperature. This is indicative of the high strain (0·34%) at the interface of bond coat/TBC at 800°C compared to the RT bend tests of the composite beam specimens [Table 2 and Fig. 4(c)]. During heating of the composite beam specimen from RT to 800°C, oxide scales on the substrate

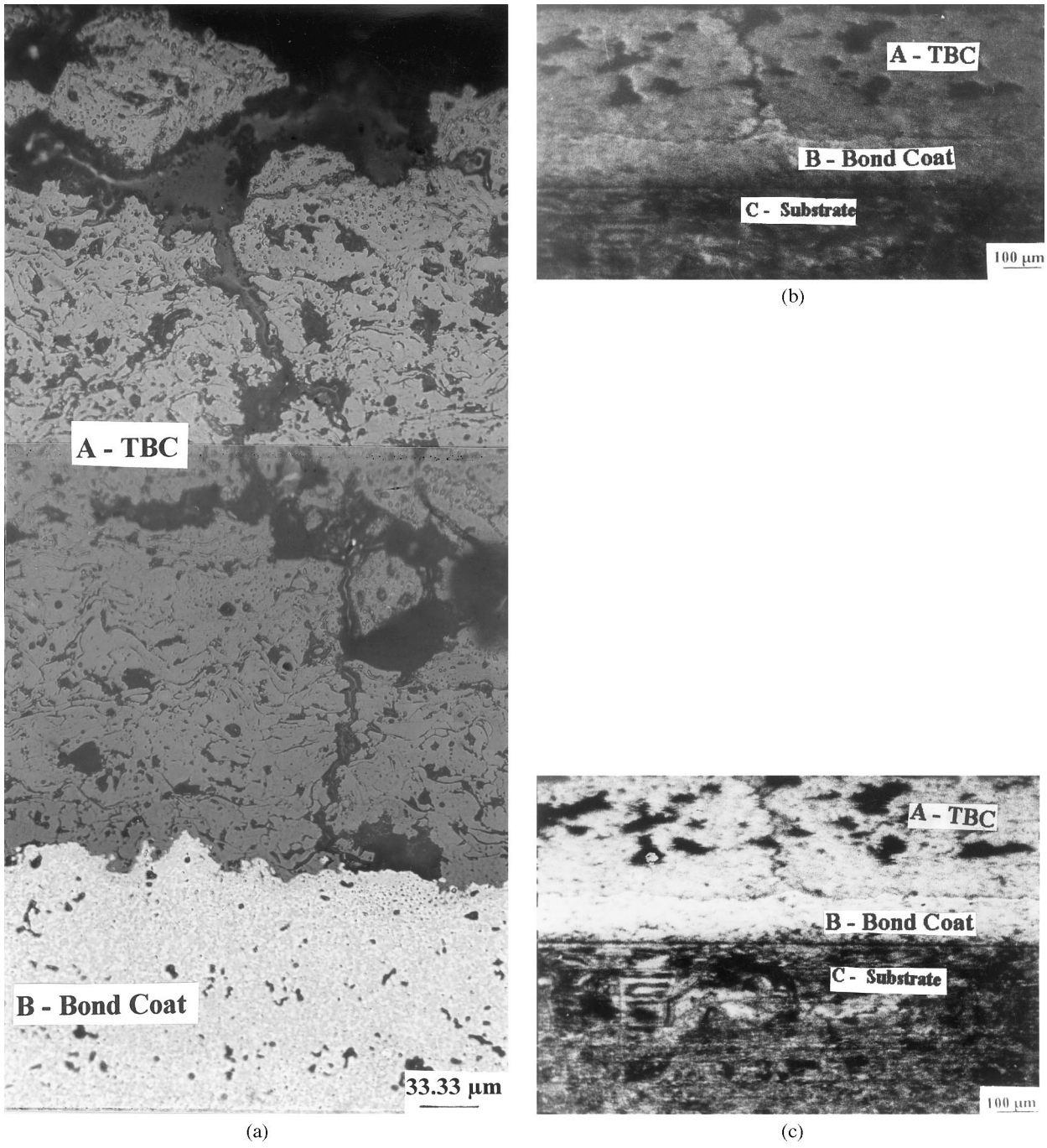

Fig. 11. (a) Typical crack path trajectory in the TBC at 800°C in type3 composite beam specimen. Crack growth at 800°C was confined only to the TBC (ceramic layer). (b) The in-situ micrograph demonstrates that crack propagation at 800°C was restricted only to the TBC (ceramic layer) in type3 composite beam specimen. (c) The crack shown in (b) is viewed at RT after cooling down of the furnace from 800°C to RT. During cooling, the TBC is under compression and the substrate under tension due to their thermal mismatch. No further crack growth was observed. The width of the crack in the TBC appears to be narrow compared to that shown in (b), possibly because the TBC is under compression during cooling.

was first observed at ~563°[2]. Subsequently with gradual change in contrast of the oxide scales on the substrate[2] from 563 to 627 to 670 to 700 to 800°C, it could be inferred qualitatively that the rate of oxidation of the substrate increased with increase in temperature. The substrate tends to expand due to its high coefficient of thermal expansion and due to the mismatch in the thermal expansion between the substrate and the TBC, it was found that above 627°C, spallation of the oxide scales were pronounced.[2] Possibly, the thermal stresses generated in the specimen were high enough to cause spallation of the oxide scales. During cooling, the crack in the TBC was also monitored which showed no increment in length. This is possibly due to compressive stresses on the ceramic layer during cooling, as a result of thermal mismatch between the substrate and the TBC.

The significant effect of oxidation on the deformation behaviour of the TBCs in the present investigation has been outlined and discussed. In Crack propagation studies it was clear that for the

oxidized sample (type2) in the TBC (ceramic layer), crack growth was noticed even at a constant load as is evident from the change in the slope of the load versu crack length curve [Fig. 6(b)]. Probably during heat treatment of the TBC (type2) at 1000°C for 200 h, the TBC/ceramic coating was densified, resulting in decrease of over all porosity. Therefore, it was assumed that the pores, i.e. the sinks for the cracks were less in number to offer any hindrance to crack propagation. As a result, crack growth was noticed within the TBC at constant load in the case of the oxidized specimens. Nevertheless, as the crack front approaches the interface of the bond coat and the ceramic layer a very threshold (load) is required [Fig. 6(b)] for the crack to penetrate and propagate in the bond coat for the oxidized sample (type2). This is mainly attributed to the microstructural toughening of the composite beam specimens due to oxidation (Fig. 2).

Previous authors have identified the mechanisms by which the first surface crack initiates on the surface of a multilayer, graded ceramic TBC.[10] Their experimental conditions were designed to simulate thermal loadings that are encountered in the combustion chamber of a diesel engine, by subjecting the surface to the heat flux until steady-state was reached, keeping it at steady-state for 2 h, and then allowing it to cool at room temperature. Cracks were formed at the surface in the region where the heat flux was concentrated. The stress distributions were calculated using the finite element method at the different stages of the thermal loading process. They have observed that surface cracks initiated in the case of zirconia coatings, from stress relaxation at high temperature, which decreased the compressive stresses due to heating over time and resulted in tensile stress upon cooling. The use of mullite, which does not relax as much as zirconia was shown to result in at least one order of magnitude increase in life of the coating.[22,23] In the case of edge crack initiation, the results showed[10] that the singular nature of the stresses does not allow a stress criterion to be used. The edge did experience both opening and shearing modes of stress intensity factors, which like surface stresses behave in a considerably different manner in diesel engines and gas turbine environments.

Thus, the design of a TBC is a complex process that has to consider the thermal loading and other conditions that can be vastly different from one application to another. The design process needs to establish criteria for acceptability from the point of view of delaying crack initiation and propagation processes. On the other hand, since the function of a TBC is to protect metallic substrates from high temperatures, the thermal resistance of the coating is also an important consideration.[10]

4 Conclusions

The aforesaid study leads to the following conclusions:

1. The crack path trajectory in the TBC (ceramic layer) often showed crack branching and crack deflection. For all composite beam specimens, the crack propagates linearly in the TBC with increase in the bending load till about the yield point of the material. Thereafter, at the interface of the TBC and the bond coat, a high threshold load is required for the crack to propagate further, in the bond coat. Once the threshold is surpassed, the crack grows rapidly into the brittle bond coat without an appreciable increase in the load.
2. Deflection versus crack length curves revealed positive linear dependence of crack length with deflection in the ceramic layer (TBC) as well as in the bond coat. It clearly infers that after the crack front penetrates the bond coat, there is a substantial amount of deflection with propagation of the crack within the bond coat, indicative of enormous plastic deformation ahead of the crack front at the interface of the bond coat and the substrate and formation of deformation twins in the metal substrate.
3. The crack front revealed blunting of the crack tip at the interface of the bond coat and the substrate indicative of high ductility of the material. It also implies that the crack to propagate further in the substrate requires a very high bending load. There was no spallation of the TBCs in either of the bend tests at RT or 800°C.
4. The strain evaluated at the interface of bond coat/TBC in the high temperature (800°C) crack propagation study, was 0·34% which is indicative of the ductility of the bond coat at 800°C compared to the brittle bond coat in the RT tests.
5. At 800°C, the crack front under bending propagated only in the TBC and not in the bond coat as the bond coat becomes ductile at high temperature and offers an attractive sink for stress relaxation.

Acknowledgements

The data presented in this paper is the outcome of a part of the project on 'Thermomechanical characterization and modelling of ceramic coatings in power plant application' at IWE-1, Jülich, Germany. This part of the programme was an Indo-German

collaboration under the bilateral exchange scheme. One of the authors, Dr Ashok K. Ray, is grateful to D.L.R. Bonn for financial support during the research stay at IWE-1, Jülich, Germany. Dr. Ray is also grateful to Professor Nickel, Professor L. Singhiser and Dr H. Schuster of IWE-1, for their moral support and encouragement. The authors are grateful to Ms G. Blandin, S. Brünnings, J. Mönch and Dr D. Basu (Central Glass and Ceramic Research Institute, Calcutta) for their assistance in the high temperature testing and to Mr Schiffers, Ms Marlise Felden and all fellow colleagues of IWE-1, Jülich, Germany for their constant encouragement.

References

1. Duret-Thual, C., Morbioli, R. and Steinmetz, P., A guide to the control of high temperature corrosion and protection of gas turbine materials. In *CEC (Commision of the European Communities) COST Energy*, ed. O. Morocutti. EUR 10682 EN, 1986. Commission of the European Communities, Brussels, Belgium.
2. Ray, A. K. and Steinbrech, R. W., Thermomechanical characterization and modelling of ceramics and coatings in powerplant applications, Internal report of (INDO-GERMAN) Collaborative Project IN-283, 1998, IWE-1, Julich, Germany.
3. Miller, R. A. and Lowell, C. E., Failure mechanisms of thermal barrier coatings exposed to elevated temperatures. *Thin Solid Films*, 1982, **95**, 265–273.
4. Brindley, W. J. and Miller, R. A., Thermal barrier coating life and isothermal oxidation of low-pressure plasma-sprayed bond coat alloys. *Surf. Coat. Technol*, 1990, **43–44**, 446–457.
5. Miller, R. A. and Berndt, C. C., Performance of thermal barrier coatings in high heat flux environments. *Thin Solid Films*, 1984, **119**, 195–202.
6. Liebert, C. H. and Miller, R. A., Ceramic thermal barrier coatings. *Ind. Eng. Chem. Prod., Res. Dev.*, 1984, **12**, 334–349.
7. DeMasi, J. T., Sheffler, K. D. and Ortiz, M., *Thermal Barrier Coating, Life Prediction Model Development*. NASA CR 182230. National Aeronautics and Space Administration, 1989.
8. Kokini, K., Choules, C. D. and Takeuchi, Y. R., Thermal fracture mechanisms in ceramic thermal barrier coatings. *J. Therm. Spray. Tech. (JTTEE) ASM International*, 1997, **6**(1), 43–49.
9. Lelait, L., Alperine, S., Diot, C. and Mevrel, M., Thermal barrier coatings: microstructural investigation after annealing. *Mater. Sci. Eng A.*, 1989, **120–121**, 475–482.
10. Kokini, K. and Takeuchi, Y. R., Initiation of surface cracks in multilayer ceramic thermal barrier coatings under thermal loads. *Mater. Sci. Eng. A.*, 1994, **189**, 301–309.
11. Sturn, K. H. (ed.) *Metallurgical and Ceramic Protective Coatings*. Chapman and Hall, London, 1996, p. 266.
12. Chiu, C. C. and Case, E. D., Elastic modulus determination of coating layers as applied to layered ceramic composites. *Mater. Sci. Eng A.*, 1991, **132**, 39–47.
13. Brandle, W., Grabke, H. J., Toma, D. and Krueger, J., The oxidation behaviour of sprayed MCrAlY coatings. *Surf. Coat. Technol.*, 1996, **86–87**, 41–47.
14. *Metals Handbook, Metallography and Microstructures*, Vol. 9, 9th edn. ASM, Metals Park, OH.
15. Timoshenko, S. P. and Young, D. H., *Strength of Materials*, 4th edn. Van Nostrand Reinhold, Princeton, NJ, 1962, p. 113.
16. Bruch, U., Schuhmacher, D., Ennis, P. J. and Heesen, E., Tensile and impact properties of candidate alloys for high-temperature gas-cooled reactor applications. *Nuclear Technol.*, 1984, **66**, 357–376.
17. Ramchandran, N. and Shetty, D. K., Rising crack growth resistance (*R*-curve) behaviour of toughened alumina and silicon nitride. *J. Am. Ceram. Soc.*, 1991, **74**(10), 2634–2641.
18. Anderson, R. M. and Braun, L. M., Technique for the *R*-curve determination of Y-TZP using indentation-produced-flaws. *J. Am. Ceram. Soc.*, 1990, **73**(10), 3059.
19. Swain, M. V., *R*-curve behaviour and thermal shock resistance of ceramics. *J. Am. Ceram. Soc.*, 1990, **73**(3), 621–628.
20. Pezzotti, G., Tanaka, I. and Okamoto, T., Si_3N_4/SiC-whisker composites without sintering Aids: II, fracture behaviour. *J. Am. Ceram. Soc.*, 1990, **73**(10), 3039–3045.
21. Ray, A. K., Fuller, E. R. and Banerjee, S., Fatigue crack growth and fracture toughness of 25 wt% silicon carbide whisker reinforced alumina composite with residual porosity. *J. Eur. Ceram. Soc.*, 1996, **16**, 503–513.
22. Takeuchi, Y. R., Kokini, K. and Yonushonis, T. M., Thermal barrier coating development for pistons. *Proc. 1992 Coatings for Advanced Heat Engines Workshop*. US Department of Energy, 1992, pp. II-31–II-40.
23. Pierz, P. M., Thermal barrier coating development for diesel engine aluminium pistons. *Surf. Coat. Technol.*, 1993, **61**, 60–66.